THE AMERICAN SOCIETY OF MECHANICAL ENGINEERS
345 E. 47th St., New York, N.Y. 10017

98-GT-113

HEAT TRANSFER IN A "COVER-PLATE" PRE-SWIRL ROTATING-DISC SYSTEM

Robert Pilbrow[1], Hasan Karabay, Michael Wilson, J Michael Owen
Department of Mechanical Engineering
Faculty of Engineering and Design
University of Bath
Bath BA2 7AY, UK

1 Now at Rolls-Royce plc, P O Box 3, Filton, Bristol BS12 7QE, UK

ABSTRACT

In most gas turbines, blade-cooling air is supplied from stationary pre-swirl nozzles that swirl the air in the direction of rotation of the turbine disc. In the "cover-plate" system, the pre-swirl nozzles are located radially inward of the blade-cooling holes in the disc, and the swirling air flows radially outwards in the cavity between the disc and a cover-plate attached to it.

In this combined computational and experimental paper, an axisymmetric elliptic solver, incorporating the Launder-Sharma and the Morse low-Reynolds-number k-ε turbulence models, is used to compute the flow and heat transfer. The computed Nusselt numbers for the heated "turbine disc" are compared with measured values obtained from a rotating-disc rig. Comparisons are presented, for a wide range of coolant flow rates, for rotational Reynolds numbers in the range 0.5×10^6 to 1.5×10^6, and for $0.9 < \beta_p < 3.1$, where β_p is the pre-swirl ratio (or ratio of the tangential component of velocity of the cooling air at inlet to the system to that of the disc). Agreement between the computed and measured Nusselt numbers is reasonably good, particularly at the larger Reynolds numbers. A simplified numerical simulation is also conducted to show the effect of the swirl ratio and the other flow parameters on the flow and heat transfer in the cover-plate system.

NOMENCLATURE

a	inner radius of disc
a_i	inner radius of cover-plate
b	outer radius of disc
C_p	specific heat at constant pressure
C_w	nondimensional flow rate $(= \dot{m} / \mu b)$
k	thermal conductivity
$\dot{m}$	mass flowrate
Nu	Nusselt number $\left(= \frac{r q_s}{k(T_s - T_{s,ad})}\right)$
Pr	Prandtl number $(= \mu C_p/k)$
Pr_t	turbulent Prandtl number
q_s	convective heat flux from disc to air
r,ϕ, z	radial, tangential and axial coordinates
R	recovery factor
Re_ϕ	rotational Reynolds number $\left(= \rho \Omega b^2 / \mu\right)$
s_1,,s_2	axial clearance in rotor-stator and rotating cavity, respectively
s	axial width of entire system
$T_{0,in}$	total temperature at inlet
T_s	surface temperature
$T_{s,ad}$	adiabatic-disc temperature $(= T_{o,in} + \Omega^2 (Rr^2 + (1 - R - 2\beta_\rho) r_p^2)/2C_p)$
U_τ	friction velocity $\left(= \sqrt{\tau_w / \rho}\right)$
V_r, V_ϕ, V_z	time-averaged radial, circumferential, axial velocity components
x	nondimensional radial coordinate (= r/b)
y	distance normal to the wall
y^+	nondimensional distance $(= \rho y U_\tau/\mu)$
β	swirl ratio $(= V_\phi/\Omega r)$
β_p	pre-swirl ratio $(= V_{\phi,p}/\Omega r_p)$
ΔT	temperature difference $(= T_s - T_{0,in})$
ε	turbulent energy dissipation rate
λ_T	turbulent flow parameter $(= C_w/Re_\phi^{0.8})$
μ	dynamic viscosity
ρ	density
τ_w	total wall shear stress
Ω	angular speed of disc

Subscripts

ad	adiabatic
b	blade-cooling air

Presented at the International Gas Turbine & Aeroengine Congress & Exhibition
Stockholm, Sweden — June 2–June 5, 1998
This paper has been accepted for publication in the Transactions of the ASME
Discussion of it will be accepted at ASME Headquarters until September 30, 1998

d	disc-cooling air
in	inlet
p	pre-swirl air
o	total temperature in stationary frame
s	surface or sealing air
t	total temperature in rotating frame

1 INTRODUCTION

Fig 1 shows a simplified diagram of a so-called cover-plate pre-swirl system that is used to supply the cooling air to the turbine blades in some gas-turbine designs. Studies of these pre-swirl systems have been carried out by many research workers, and the reader is referred to Meierhofer and Franklin (1981), El-Oun and Owen (1989), Chen *et al* (1993a, b), Popp *et al* (1996), Wilson *et al* (1997) and Karabay *et al* (1997). Further details of these and other rotating-disc systems are given by Owen and Rogers (1989, 1995).

The cooling air is supplied from stationary pre-swirl nozzles, at a radial location of $r = r_p$, that swirl the air in the direction of rotation of the turbine disc, or rotor in Fig 1. At $r = r_p$, the swirl ratio, β_p, which is the ratio of the tangential component of velocity of the air, $V_{\phi,p}$, to that of the disc, Ωr_p, is usually greater than unity. The swirling air then flows radially outward, in the space between the rotor and a cover-plate attached to it, to leave the system through blade-cooling passages in the disc at $r = r_b$. By swirling the cooling air, its temperature is reduced relative to the rotating passages, with consequent advantages for the blade-cooling system.

Some of the pre-swirl air is allowed to leak radially outwards through the seal between the rotating cover-plate and the stator, as shown in Fig 1. This sealing air helps to prevent or reduce the ingress of hot mainstream gas into the cooling system, and it also removes the "windage heating" that is generated by the rotating cover-plate.

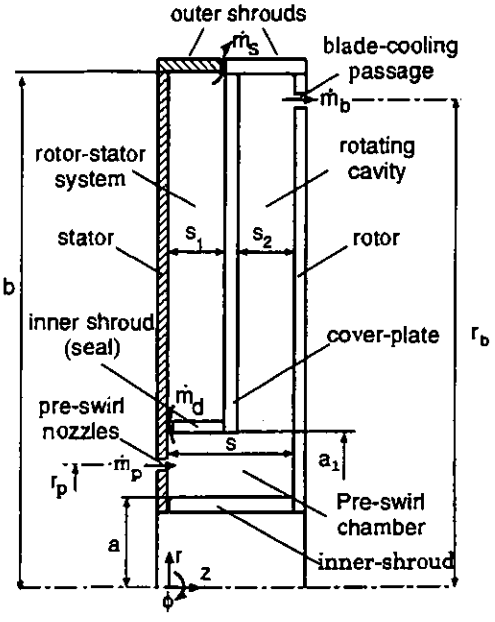

Fig 1 Simplified diagram of cover-plate pre-swirl system

The complete system shown in Fig 1 can be considered as two sub-systems : a rotor-stator system and a rotating cavity (see Owen and Rogers 1989, 1995). A combined theoretical, computational and experimental study of the flow in an adiabatic cover-plate system was conducted by Karabay *et al* (1997), who showed that the flow in the rotating cavity was not affected by that in the rotor-stator system. The flow in the rotating cavity is mainly controlled by two parameters: β_p and $\lambda_{T,b}$, where $\lambda_{T,b}$, is the turbulent flow parameter defined as

$$\lambda_{T,b} = C_{w,b}\ Re_\phi^{-0.8} \tag{1.1}$$

$C_{w,b}$ is the nondimensional flow rate of the blade-cooling air and Re_ϕ is the rotational Reynolds number defined in the nomenclature.

The flow structure in a rotating cavity comprises a number of regions (see Owen and Rogers 1995): there are boundary layers on the two discs and the outer shroud, between which there is a core of rotating fluid. For small values of $\lambda_{T,b}$, the core will comprise two regions: a source region at the smaller radii, in which flow is entrained into the boundary layers on the discs, and an inviscid core between the nonentraining Ekman-type boundary layers. The source region extends radially to the point where all superposed flow has been entrained into the boundary layers. For sufficiently large flow rates or, more precisely, for sufficiently large values of $\lambda_{T,b}$, the source region fills the entire space between the boundary layers in the cavity.

Inside the source region, angular momentum is conserved and a free vortex is formed outside the boundary layers such that

$$\frac{V_\phi}{\Omega r} = \beta_p \left(\frac{x_p}{x}\right)^2 \tag{1.2}$$

Owen and Rogers also suggested that, providing $\beta_p\ x_p^2 < 1$, the source region would fill the cavity when

$$\lambda_{T,b} = 0.437\,(1 - (\beta_p\ x_p^2)^{1.18})^{1.66} \tag{1.3}$$

For $\lambda_{T,b}$ greater than this value, or when $\beta_p\ x_p^2 > 1$, equation (1.2) should apply throughout the cavity, outside of the boundary layers; for smaller values of $\lambda_{T,b}$, Ekman-type layers will form on the discs and angular momentum will not be conserved in the core.

Karabay *et al* computed the flow structure and compared the computed tangential components of velocity in the cover-plate system with measured values. They showed that, for sufficiently large values of $\lambda_{T,b}$, there is free-vortex flow between the cover-plate and the disc, and their computations were in good agreement with the measured velocities. As the computations were made using an axisymmetric solver (see Section 2), the good agreement between the computed and measured velocities suggests that the three-dimensional effects associated with discrete pre-swirl nozzles have little influence on the flow between the cover-plate and the rotor.

In this paper, the adiabatic study of Karabay *et al* is extended to include heat transfer from the disc to the cooling air, and measurements made in an experimental rig are compared with computations made with an elliptic solver. A separate "parametric study" is also carried out computationally for the rotating cavity, so that the effects of Re_ϕ, $C_{w,b}$, $\lambda_{T,b}$ and β_p on the flow structure and heat transfer can be examined. The computational method is outlined in Section 2, and the experimental rig is described in Section 3. In Section 4, the parametric study is discussed, in Section 5 the computed and measured Nusselt numbers are compared, and the conclusions are summarised in Section 6.

2 COMPUTATIONAL MODEL

The steady-state, axisymmetric finite-volume solver used in this work is the same as that described by Karabay *et al* (1997) for a study of the flow structure.

Turbulent flow computations were made using both the low-Reynolds-number k-ε models of Launder-Sharma (1974) and of Morse (1988), the latter incorporating modifications suggested by its author (Chen *et al* 1996). Incompressible flow was assumed and turbulent heat transfer was represented using a turbulent Prandtl number Pr_t equal to 0.9.

A staggered grid was used with the axial and radial velocity components stored mid-way between the grid points where other solution variables were located (pressure, tangential velocity, turbulence kinetic energy and dissipation rate, and total enthalpy). The cover-plate and inner shroud (see Fig. 1) were represented by block obstructions within the computational grid and the equations were solved using the SIMPLEC pressure-correction algorithm.

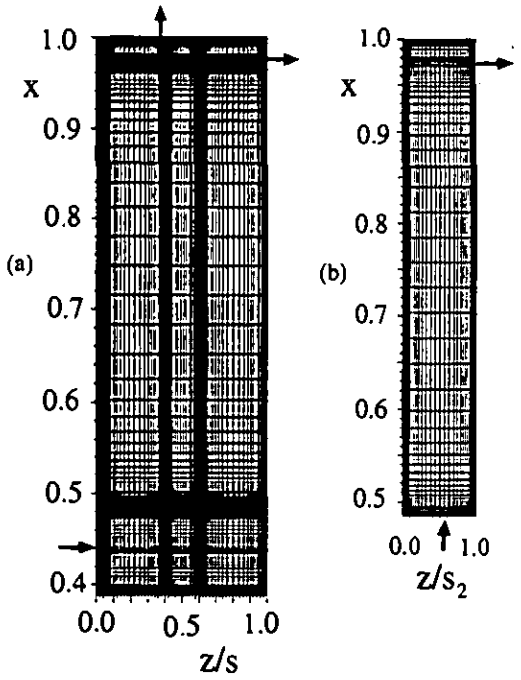

Fig 2 Grid distribution used in computation
a) Complete system b) Simple cavity

The inlet nozzles and blade-cooling holes of the experimental rig were represented in the axisymmetric model by equivalent-area annular slots on the stator and rotor, with centrelines at $r = r_p$ and $r = r_b$ respectively. The axial velocity V_z of the pre-swirl air, which was assumed uniform at the inlet, was deduced from the prescribed mass flow rate $\dot{m}_p$. Similarly, the axial velocity at the blade-cooling slot and the radial velocity at the outer seal were calculated from mass flow rates $\dot{m}_b$ and $\dot{m}_s$ respectively; global mass balance was achieved by ensuring that $\dot{m}_p = \dot{m}_b + \dot{m}_s$. The inlet tangential velocity $V_{\phi,p}$ was fixed to give the required swirl ratio β_p, and Neumann (zero normal-derivative) boundary conditions for V_ϕ were used at the two outlets. The remaining velocity components at flow boundaries were taken to be zero, and no-slip conditions were applied at all solid surfaces. The temperatures of the pre-swirl air and the heated rotating disc were taken from the measured values, the other solid surfaces were assumed to be adiabatic, and zero-derivative conditions were used at both outlets.

The turbulence models required a very fine grid near the boundaries, with $y+ < 0.5$ for the near-wall grid nodes, and the grid-spacing increased geometrically away from walls (including the cover-plate and shroud) with expansion factors of about 1.2. A 223 by 223 axial by radial grid was used for the whole system, and for the simple cavity a 67 by 111 axial by radial grid was used (see Fig 2). Eight points covered the inlet and blade-cooling slots. (Computations were also conducted with a 141 x 185 grid. This made no significant difference to the comparison between the computed and measured Nusselt numbers, which suggests that the results presented below are sensibly grid-independent.)

About 55 axial grid nodes were located within the cover-plate, with the remaining points divided equally between the rotor-stator system and the rotating cavity; about 70 grid points covered the annular pre-swirl chamber (see Fig. 1).

Convergence of the iterative method was improved using the Gosman distributive damping term and a fixed V-cycle multigrid algorithm. Computation times, using a Silicon Graphics R10000 processor, were typically around 12 hours for the whole cavity and two hours for the simple cavity.

3 EXPERIMENTAL APPARATUS

The apparatus is the same as that used by Karabay *et al* (1997) for their adiabatic study. A schematic diagram is shown in Fig 1, and details of the rotating-disc rig are shown in Fig 3.

The outer radius of the system, b, was approximately 207 mm, and the radial location of the pre-swirl nozzles and blade-cooling holes were r_p = 90 mm and r_b = 200 mm. There were 19 pre-swirl nozzles of 7.92 mm diameter, angled at 20° to the tangential direction, and 60 blade-cooling holes of 7.7 mm diameter, with their axes normal to the disc. The axial spacing between the cover-plate, which was 5 mm thick, and the stator, s_1, was 10 mm, and between the cover-plate and the rotor the spacing, s_2, was also 10 mm. The inner radius, a, and outer radius, a_1, of the annular pre-swirl chamber were 80 mm and

100 mm, and air entered the rotating cavity through the annular clearance at the centre of the cover-plate.

The mass flow rates of the pre-swirl, blade-cooling and sealing flow, $\dot{m}_p$, $\dot{m}_b$ and $\dot{m}_s$, respectively, could be independently controlled, and the flow rates were measured, with an uncertainty of ± 3% by orifice plates made to British Standards (BS1042). The rotor assembly could be rotated up to 7000 rev/min by a variable-speed electric motor, and the speed could be measured with an uncertainty of ± 1 rev/min. (For the tests conducted on this rig, a speed of 7000 rev/min corresponds to $Re_\phi \cong 2.4 \times 10^6$.)

The front (cavity-side) face of the heated rotor was covered in a fibre-glass "mat", 1-mm thick, in which ten thermocouples and six fluxmeters were embedded. It should be pointed out that the instrumentation had been installed on the rotating disc for the earlier tests with a direct-transfer pre-swirl system (see Wilson *et al* 1997). Three of the thermocouples were placed in the heated outer part of the disc, and one of the fluxmeters was located underneath the carbon-fibre ring that connected the outside of the cover-plate to this disc. Consequently, only seven thermocouples and five fluxmeters were located in the test-section of the cover-plate system. Unfortunately, none of the fluxmeters was located at the radius of pre-swirl nozzles. Details of the RdF thermopile fluxmeters and their calibration are given by Wilson *et al* (1997).

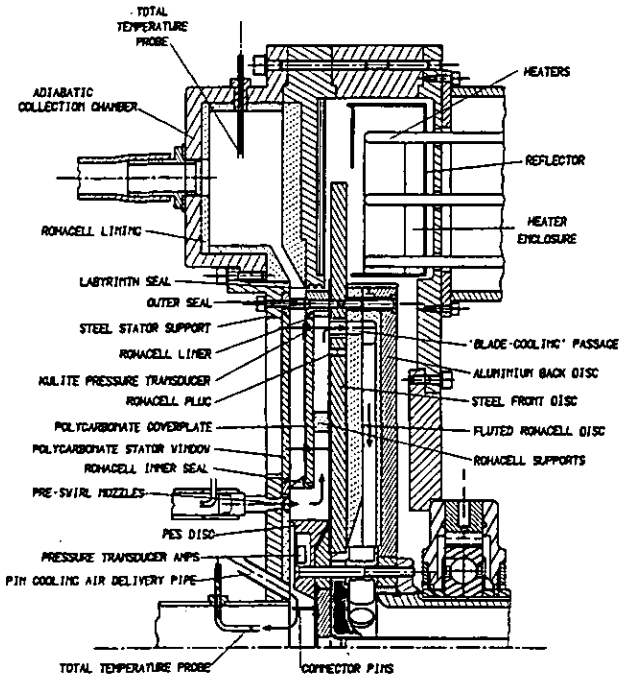

Fig 3 Details of rotating-disc rig

In addition, total-temperature thermocouple probes were located in two of the blade-cooling holes in the disc. (The measurements of the temperature of the blade-cooling air will be reported in a future paper.) The signals from all the rotating instrumentation were brought out through a 24-channel silver/silver-graphite slipring unit, and the voltages were measured with an uncertainty of ±1μV by a computer-controlled Solartron data logger.

The outer part of the rotating disc was heated up to 150°C by means of stationary radiant electric heater units, with a maximum power output of 9.5kW. The actual temperature distribution over the instrumented section of the disc depended on the rotational speed and on the flow rate of the cooling air, and the maximum temperature in this section was typically around 70°C. The temperature of the air at the pre-swirl nozzles, which was measured with two total-temperature probes, was controlled by a heat exchanger to between 10°C and 20°C. The outlet temperature of the cooling air in the rotor-stator system was measured by two total-temperature probes in the adiabatic collection chamber.

The cover-plate was made from transparent polycarbonate ($k \cong 0.2$ W/mK) giving optical access for LDA measurements. Segments of both surfaces of the cover-plate and the front surface of the heated disc were coated with thermochromic liquid crystal, which enabled the temperature to be estimated. The periphery of the cover-plate was attached to the disc by a carbon-fibre ring, the inner surface of which was insulated with a Rohacell-foam liner ($k \cong 0.03$ W/m K); the cover-plate itself was quasi-adiabatic. The axial spacing between the cover-plate and the disc was maintained by six supports, made from Rohacell foam.

For a typical engine, $Re_\phi \cong 10^7$, $\lambda_{T,b} \cong 0.3$, $\beta_p \cong 2.5$. For the heat transfer tests in the rig, the following range of parameters was tested: $0.5 \times 10^6 < Re_\phi < 1.6 \times 10^6$, $0.16 < \lambda_{T,b} < 0.32$, $0.9 < \beta_p < 3.1$. It should be pointed out that, as $\beta_p \propto C_{w,p}/Re_\phi$ and $C_{w,p} = C_{w,b} + C_{w,s}$, it is possible to keep $C_{w,b}$ and Re_ϕ constant and to vary β_p by varying $C_{w,s}$.

4 PARAMETRIC STUDY OF SIMPLE ROTATING CAVITY

For this computational study, which was made using the Morse turbulence model, the geometry was based on the rotating cavity between the cover-plate and rotor of the rotating-disc rig described in Section 3. The following range of parameters was used:

$s_z/b = 0.048$, $a/b = 0.48$, $r_b/b = 0.97$
$0.5 \times 10^6 < Re_\phi < 3.6 \times 10^6$
$8730 < C_{w,b} < 26180$
$0.1 < \lambda_{T,b} < 0.3$
$0.75 < \beta_p < 3.0$

Unlike the rig, where the flow entered the cavity axially, the flow in this model entered radially at $r = a_1$ with $V_\phi = \beta_p \Omega a_1$, and left axially through an annular slot at $r = r_b$. Details of the computational model are given in Section 2, and the computational grid is shown in Fig 2b.

Fig 4 shows the computed streamlines for six different sets of flow parameters. Figs 4a and 4b show the effect of $\lambda_{T,b}$ (or $C_{w,b}$) when Re_ϕ and β_p are held constant; Figs 4c and 4d show the effect of Re_ϕ (or $\lambda_{T,b}$) when $C_{w,b}$ and β_p are constant; Figs 4e and 4f show the effect of β_p when Re_ϕ and $C_{w,b}$ (and consequently $\lambda_{T,b}$) are constant.

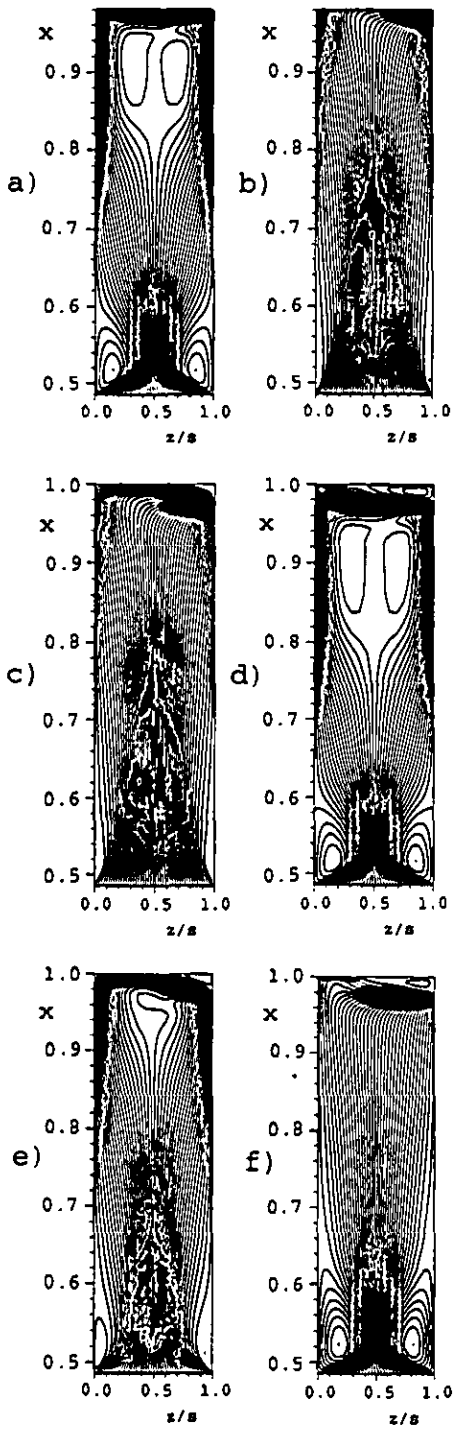

Fig 4 Computed streamlines in simple cavity

a) $Re_\phi = 1.5 \times 10^6$, $C_{w,b} = 8730$, $\lambda_{T,b} = 0.1$, $\beta_p = 1.5$
b) $Re_\phi = 1.5 \times 10^6$, $C_{w,b} = 26180$, $\lambda_{T,b} = 0.3$, $\beta_p = 1.5$
c) $Re_\phi = 0.9 \times 10^6$, $C_{w,b} = 17455$, $\lambda_{T,b} = 0.3$, $\beta_p = 1.5$
d) $Re_\phi = 3.56 \times 10^6$, $C_{w,b} = 17455$, $\lambda_{T,b} = 0.1$, $\beta_p = 1.5$
e) $Re_\phi = 1.5 \times 10^6$, $C_{w,b} = 17455$, $\lambda_{T,b} = 0.2$, $\beta_p = 1.5$
f) $Re_\phi = 1.5 \times 10^6$, $C_{w,b} = 17455$, $\lambda_{T,b} = 0.2$, $\beta_p = 3.0$

Referring to Fig 4a, the following points should be noted:

(i) Recirculation occurs in the separation zone on both discs up to $x \cong 0.58$. In source-sink flow in rotating cavities, radial outflow occurs in the boundary layers on the discs where $V_\phi/\Omega r < 1$, and inflow occurs where $V_\phi/\Omega r > 1$ (see Owen and Rogers 1995). For $\beta_p = 1.5$, $V_\phi/\Omega r = 1$ at $x \cong 0.58$; this marks the border between inflow and outflow in the boundary layers.

(ii) According to equation (1.3), for $\beta_p = 1.5$ and $Re_\phi = 1.5 \times 10^6$, the source region fills the cavity when $\lambda_{T,b} \geq 0.25$. This implies that, for $\lambda_{T,b} = 0.1$, Ekman-type layers will occur at the larger radii, as is indeed shown in Fig 4a where the source region ends at $x \cong 0.83$.

(iii) Half the fluid flows up the left-hand disc and separates from the shroud, at $x = 1$, to form a free shear layer that flows axially out through the exit slot in the right-hand disc. The other half of the fluid flows up the right-hand disc to mix with that from the left-hand disc in the exit slot.

Fig 4b shows no sign of Ekman-type layers: for $Re_\phi = 1.5 \times 10^6$ and $\beta_p = 1.5$, a value of $\lambda_{T,b} = 0.3$ ensures source flow throughout the cavity, which is consistent with equation (1.3).

The flow structure for Fig 4c is virtually the same as for Fig 4b. For both these figures, $\beta_p = 1.5$ and $\lambda_{T,b} = 0.3$; even though the values of $C_{w,b}$ and Re_ϕ are different, the values of $\lambda_{T,b}$ are the same. The same observation about similar flow structures can be made for Figs 4d and 4a where $\beta_p = 1.5$ and $\lambda_{T,b} = 0.1$. This supports the statement that, for a given value of β_p, the flow structure depends principally on $\lambda_{T,b}$.

Figs 4e and 4f show the effect of β_p on the flow structure for the case where $\lambda_{T,b} = 0.2$. For $Re_\phi = 1.5 \times 10^6$, equation (1.3) gives $\lambda_{T,b} = 0.25$ for $\beta_p = 1.5$ and 0.078 for $\beta_p = 3$. These results are consistent with the fact that the source region shown in Fig 4e does not fill the cavity and that in Fig 4f does.

Figs 5a, 5b and 5c show the effects of $\lambda_{T,b}$ and β_p on the computed Nusselt numbers for the heated disc. (For the Nusselt numbers presented in this paper, the adiabatic-disc temperature was derived from Owen and Rogers 1995.)

Referring to Fig 5a, it can be seen that there are large peaks in Nu near the inlet at $x = 0.48$, near the edge of the separation zone at $x \cong 0.58$ and near the outlet at $x \cong 0.97$. Large values of Nu are expected in these regions, where the boundary layers are very thin, but the computed magnitudes, which depend on the turbulence model, are unlikely to be correct. For $\lambda_{T,b} = 0.2$ and 0.3, Nu increases with x for $0.7 \leq x \leq 0.97$. This is in the source region where cold fluid is entrained into the boundary layers on the discs: the heated disc behaves in a similar way to a free disc where Nu increases as x increases. The curve for $\lambda_{T,b} = 0.1$ departs from those for $\lambda_{T,b} = 0.2$ and 0.3 at $x \cong 0.82$, which is the start of the Ekman-type layers shown in Fig 4a: in these nonentraining layers, the fluid heats up as it flows radially outward, and the heat transfer drops below that in the entraining layers.

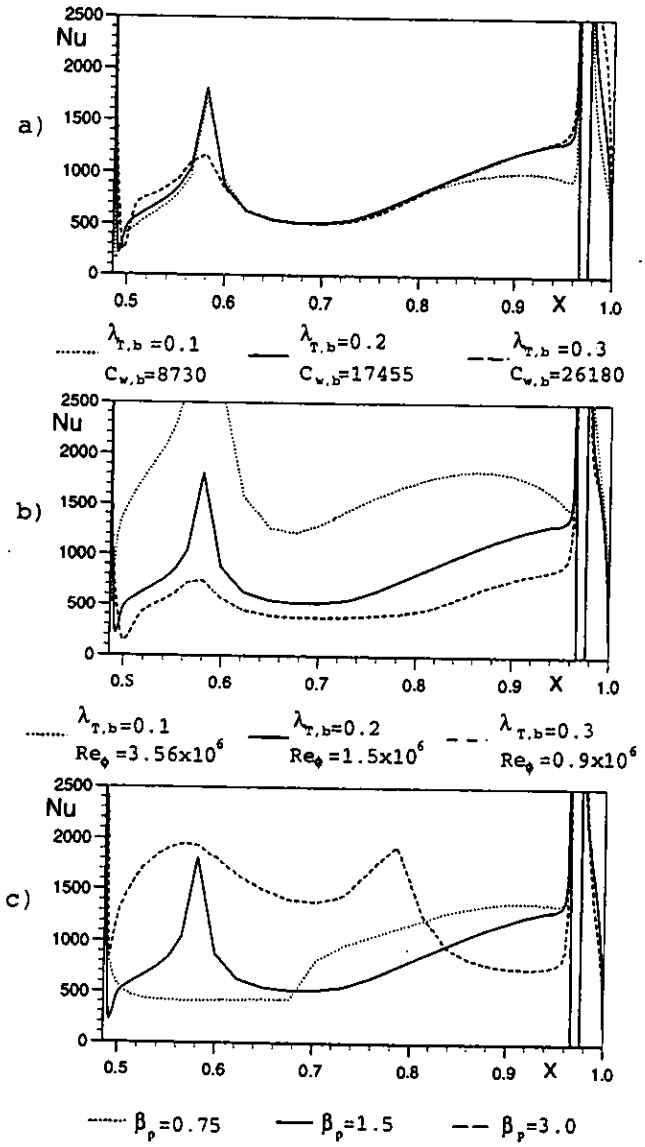

Fig 5 Computed Nusselt numbers in simple cavity

a) Effect of $\lambda_{T,b}$ for $Re_\phi = 1.5 \times 10^6$ and $\beta_p = 1.5$
b) Effect of Re_ϕ for $C_{w,b} = 17455$ and $\beta_p = 1.5$
c) Effect of β_p for $Re_\phi = 1.5 \times 10^6$, $C_{w,b} = 17455$ ($\lambda_{T,b} = 0.2$)

Fig 5b shows the three peaks in Nu referred to above but there is a significant effect of Re_ϕ : Nu increases as Re_ϕ increases. In particular, for $\lambda_{T,b} = 0.1$ and $\beta_p = 1.5$, comparison between Figs 5a and 5b shows that Re_ϕ is much more significant than $C_{w,b}$ in its effect on Nu : for a given value of β_p , $\lambda_{T,b}$ has the most significant effect on flow structure but Re_ϕ has the most significant effect on Nu. Again, for $\lambda_{T,b} = 0.1$ and $Re_\phi = 3.56 \times 10^6$, the decay in Nu for $x \cong 0.85$ is associated with the formation of Ekman-type layers on the heated disc.

Fig 5c shows the effect of β_p on Nu. For $\beta_p = 0.75$, where the flow in the boundary layers is radially outward and there is no recirculation zone near the centre, there appears to be transition from laminar to turbulent flow at $x \cong 0.68$ where $x^2\, Re_\phi = 6.9 \times 10^5$. For $\beta_p = 1.5$ and 3.0, the reattachment points occur at $x \cong 0.58$ and 0.78 respectively; these mark the points where the respective maxima in Nu occur in Fig 5c. It can be seen that, for a given value of $\lambda_{T,b}$, β_p has a significant effect on the distribution of Nu.

The following tentative conclusions are drawn about the flow and heat transfer in the simple rotating cavity:

(i) The flow structure depends strongly on $\lambda_{T,b}$ and β_p .

(ii) For $\lambda_{T,b}$ large enough to ensure that the source region fills the entire cavity, Nu is virtually independent of $\lambda_{T,b}$ but depends strongly on Re_ϕ and β_p.

(iii) There are peaks in Nu near the inlet, near the reattachment point (for $\beta_p > 1$), and near the exit.

5 COMPARISON BETWEEN COMPUTED AND MEASURED NUSSELT NUMBERS

In Section 4, the computed flow streamlines and Nusselt numbers were presented for the simple cavity where the flow enters radially. In the experiments, the swirling flow leaves the pre-swirl nozzles axially and enters the rotating cavity as shown in Fig 6, where $Re_\phi = 1.52 \times 10^6$, $C_{w,b} = 1.55 \times 10^4$, $\lambda_{T,b} = 0.17$ and $\beta_p = 1.65$; this corresponds to one of the test cases discussed below. (Karabay *et al* 1997 include details of the computed flow structures for a range of conditions.)

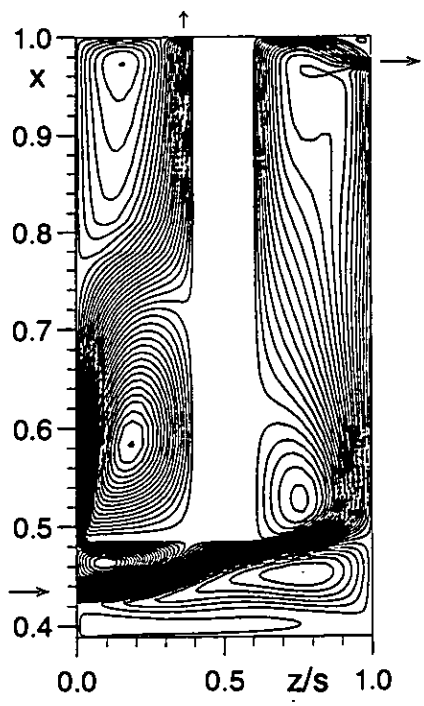

Fig 6 Computed streamlines for cover-plate pre-swirl system: $Re_\phi = 1.52 \times 10^6$, $C_{w,b} = 1.55 \times 10^4$, $\lambda_{T,b} = 0.17$ and $\beta_p = 1.65$

Referring to Fig 6, the rotor-stator system (which is not discussed here) is on the left and the rotating cavity on the right. A swirling jet of fluid (with β_p = 1.65) flows axially from the pre-swirl nozzles at x_p = 0.44 and impinges on the rotor at x ≅ 0.5; for x < 0.5 the flow on the rotor is radially inward, and for x > 0.5 it is radially outward. The flow separates from the edge of the cover plate, forming a recirculation zone, and reattaches at x ≅ 0.6. For these conditions, the source region does not fill the cavity, and there are signs of Ekman-type layers for x > 0.85.

Compared with the simple cavity, the flow is similar at the larger radii (see, for example, Fig 4e) but differs significantly at the smaller radii. In particular, the flow near the impingement point on the rotor is significantly different from that in the simple cavity; the computed radial location of this impingement point is virtually invariant with $\lambda_{T,b}$ and β_p.

Comparisons between the computed and measured Nusselt numbers are shown in Figs 7 to 10. Also shown are the measured values of ΔT (where $\Delta T = T_s - T_{0,\,in}$), and the fitted curve, which was used to provide the thermal boundary conditions for the rotor surface in the computations; the other surfaces were assumed to be adiabatic. For the computations, both the Launder-Sharma and Morse turbulence models were used, as described in Section 2.

Fig 7 shows the effect of β_p on Nu for $Re_\phi \cong 0.5 \times 10^6$ and $\lambda_{T,b}$ ≅ 0.17; as discussed in Section 3, β_p was varied by varying $C_{w,s}$ whilst keeping $\lambda_{T,b}$ approximately constant. The following observations can be made:

(i) There is a peak in the computed Nusselt numbers at x ≅ 0.5 for all cases, which corresponds to the impingement region referred to above. Unlike the results for the simple cavity shown in Fig 5, there is no peak in Nu at x = 0.4; this is a direct result of the difference between the radial and axial inlets for these two configurations. (Unfortunately, as stated in Section 3, there are no fluxmeters in this inner region.)

(ii) There are computed peaks near the outlet at x ≅ 0.97, as also observed in the simple cavity. In the axisymmetric computations, the blade-cooling holes were modelled as an equivalent-area annular slot, and so the heat transfer in this region is not directly comparable with the measurements, which were obtained in the area between the blade-cooling holes. However, the measurements do show a significant increase in Nu in this region, and the magnitude is approximately double that of the measured values at the other radii. The flow and heat transfer in the region around the holes is highly three-dimensional and cannot be simulated by an axisymmetric solver

(iii) Between these two peaks, the computed Nusselt numbers show similar trends to the measured values. Both turbulence models tend to underestimate the measurements, although the Morse model shows much closer agreement than the Launder-Sharma model. As there are no experimental data in the impingement region, it is not possible to comment on the relative performance of the two models in this area. (As the Morse model shows better agreement with all the data presented here, only that model will be mentioned in the following discussion.)

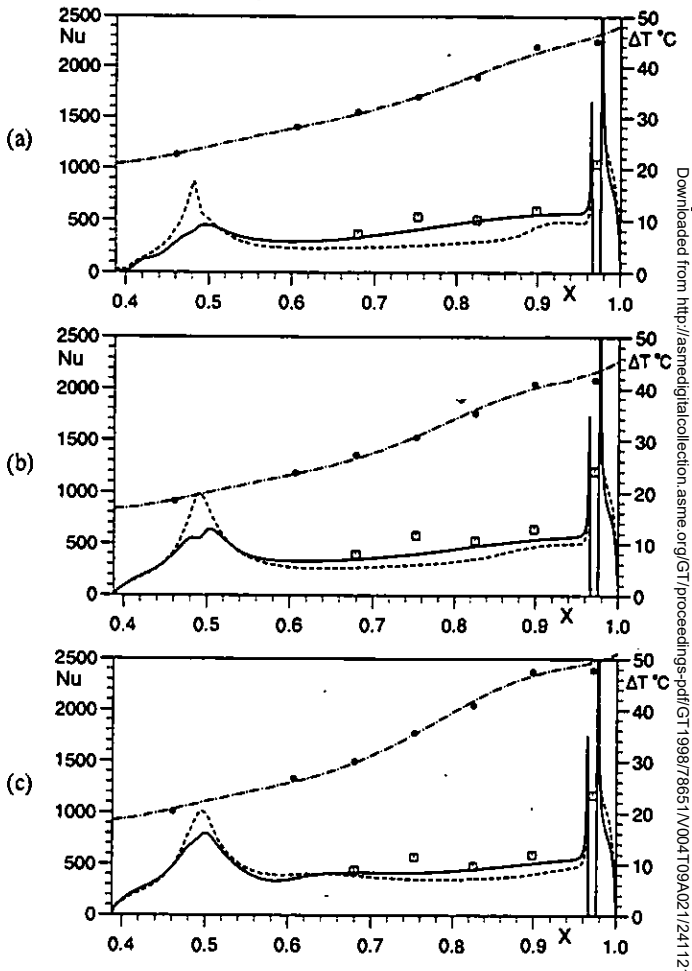

Fig 7 Comparison between computed and measured Nusselt numbers for $Re_\phi \cong 0.5 \times 10^6$ and $\lambda_{T,b} \cong 0.17$

□ measured Nu. ● measured ΔT; — · — fitted ΔT,
---- computed Nu (LS model); —— computed Nu (Morse model)

a) $Re_\phi = 0.535 \times 10^6$, $C_{w,b} = 6636$, $\lambda_{T,b} = 0.173$, $\beta_p = 1.11$
b) $Re_\phi = 0.542 \times 10^6$, $C_{w,b} = 6785$, $\lambda_{T,b} = 0.176$, $\beta_p = 1.54$
c) $Re_\phi = 0.559 \times 10^6$, $C_{w,b} = 7005$, $\lambda_{T,b} = 0.177$, $\beta_p = 2.01$

Fig 8 shows the effect of β_p for $Re_\phi \cong 1.5 \times 10^6$ and $\lambda_{T,b} \cong 0.17$. As stated above, the value of β_p does not significantly affect the radial location of the impingement region, but it does affect the magnitude of Nu in this region. It can be seen that, for the larger value of Re_ϕ, the agreement between the measured and computed Nusselt numbers, using the Morse model, is good. Comparison between Figs 7 and 8 shows that Nu increases as Re_ϕ increases, as was found for the simple cavity.

Fig 9 shows the effect of β_p for $Re_\phi \cong 0.5 \times 10^6$ and $\lambda_{T,b} \cong 0.35$; the value of Re_ϕ is similar to that in Fig 7 but the value of $\lambda_{T,b}$ is double. The computations show little effect of β_p and are in reasonable agreement with the experimental data, except for the

case shown in Fig 9c, where $\beta_p = 3.06$; for this case, the measured Nusselt numbers are significantly higher than the computed values.

Fig 10 shows the effect of β_p for $Re_\phi \cong 1.2 \times 10^6$ and $\lambda_{T,b} \cong 0.35$; the value of Re_ϕ is similar to that in Fig 8 but the value of $\lambda_{T,b}$ is double. Again the agreement between the computed and measured values of Nu is reasonable. Comparison between Figs 9 and 10 shows that increasing Re_ϕ has, as noted above, a significant effect on the magnitude of Nu.

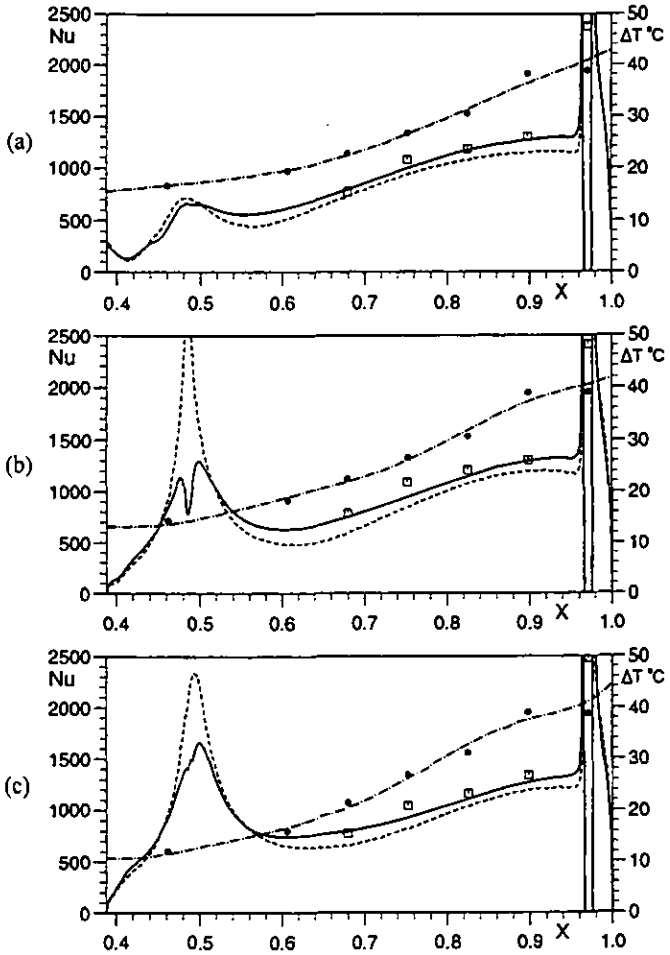

Fig 8 Comparison between computed and measured Nusselt numbers for $Re_\phi \cong 1.5 \times 10^6$ and $\lambda_{T,b} \cong 0.17$
(For legend, see Fig 7)

a) $Re_\phi = 1.41 \times 10^6$, $C_{w,b} = 14411$, $\lambda_{T,b} = 0.174$, $\beta_p = 0.91$
b) $Re_\phi = 1.41 \times 10^6$, $C_{w,b} = 14411$, $\lambda_{T,b} = 0.174$, $\beta_p = 0.91$
c) $Re_\phi = 1.52 \times 10^6$, $C_{w,b} = 15514$, $\lambda_{T,b} = 0.176$, $\beta_p = 1.65$

6 CONCLUSIONS

(i) A computational parametric study of the effects of Re_ϕ, $C_{w,b}$, $\lambda_{T,b}$ and β_p on the flow and heat transfer in a simple rotating cavity with a radial inlet shows conventional source-sink flow where the size of the source region depends on $\lambda_{T,b}$ and β_p. For large values of $\lambda_{T,b}$, the source region can fill the entire cavity outside the (entraining) boundary layers on the discs and shroud. For small values of $\lambda_{T,b}$, where the

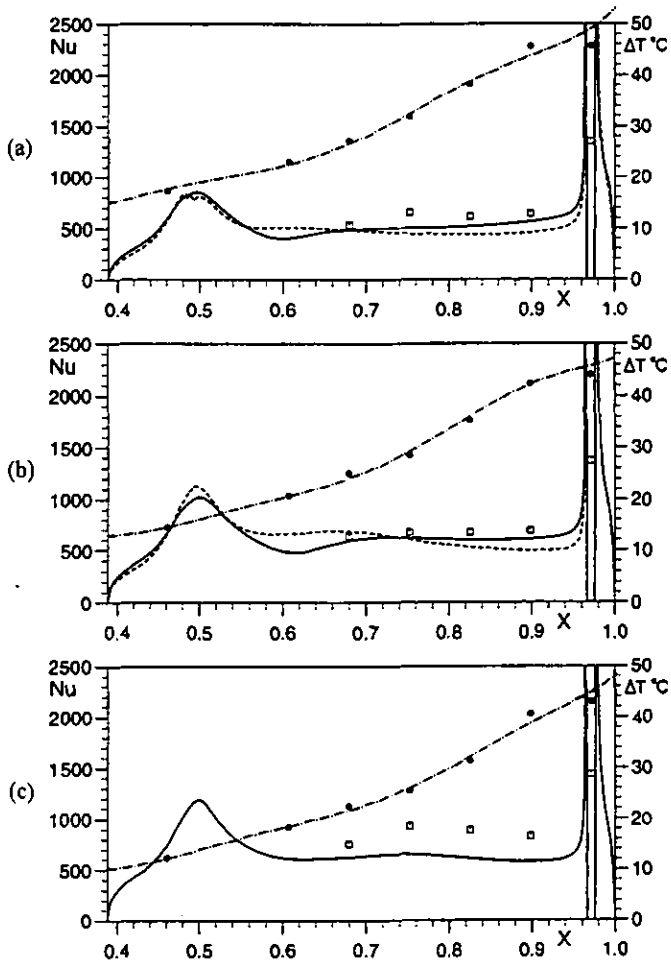

Fig 9 Comparison between computed and measured Nusselt numbers for $Re_\phi \cong 0.5 \times 10^6$ and $\lambda_{T,b} \cong 0.35$
(For legend, see Fig 7)

a) $Re_\phi = 0.569 \times 10^6$, $C_{w,b} = 14068$, $\lambda_{T,b} = 0.350$, $\beta_p = 2.24$
b) $Re_\phi = 0.569 \times 10^6$, $C_{w,b} = 14162$, $\lambda_{T,b} = 0.352$, $\beta_p = 2.53$
c) $Re_\phi = 0.588 \times 10^6$, $C_{w,b} = 14562$, $\lambda_{T,b} = 0.353$, $\beta_p = 3.06$

source region does not fill the cavity, (nonentraining) Ekman-type layers form on the rotating discs. Owing to the fact that the fluid in the nonentraining layers heats up as it flows radially outward, the Nusselt numbers in these layers tend to be lower than those in the entraining layers

(ii) The computations show that the Nusselt numbers on the heated rotor depend principally on Re_ϕ, $\lambda_{T,b}$ and β_p.

(iii) The agreement between the measured Nusselt numbers and the axisymmetric computations using the Morse turbulence model is reasonably good, particularly at the larger values of Re_ϕ. The Launder-Sharma model tends to underpredict the measured data.

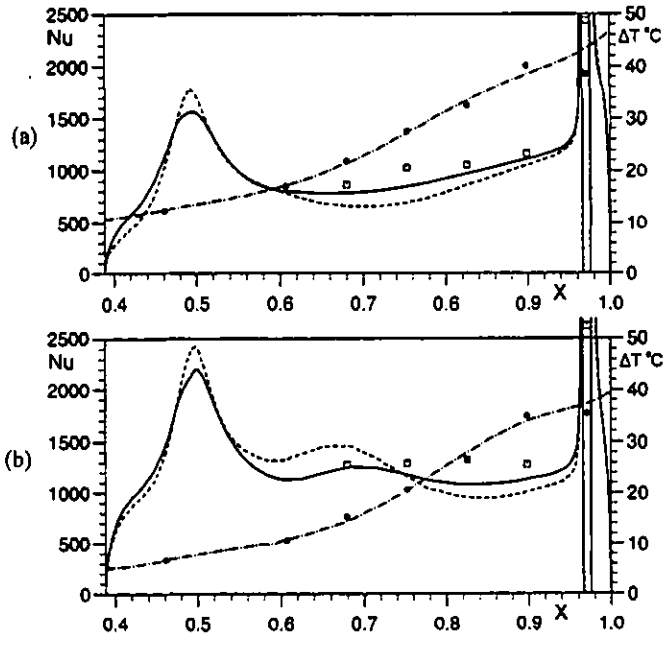

Fig 10 Comparison between computed and measured Nusselt numbers for $Re_\phi \cong 1.2 \times 10^6$ and $\lambda_{T,b} \cong 0.35$ (For legend, see Fig 7)

a) $Re_\phi = 1.22 \times 10^6$, $C_{w,b} = 25953$, $\lambda_{T,b} = 0.351$, $\beta_p = 1.90$
b) $Re_\phi = 1.37 \times 10^6$, $C_{w,b} = 28354$, $\lambda_{T,b} = 0.349$, $\beta_p = 2.61$

(iv) The computations show peaks in Nu in the region where the pre-swirl flow impinges on the rotor and in the region around the blade-cooling slot; measurements of Nu were not made in the impingement region, but those made near the blade-cooling holes in the rig showed a peak value approximately double that of the measurements at smaller radii.

The study reported in this paper has concentrated principally on the local Nusselt numbers. These obviously have a significant effect on the temperature of the blade-cooling air, and this will be the subject of a future paper on the cover-plate pre-swirl system.

ACKNOWLEDGEMENTS

The authors thank the Engineering and Physical Sciences Research Council and European Gas Turbines Ltd for funding the research described in this paper, and the Turkish Government and Kocaeli University for providing the financial support for Hasan Karabay.

REFERENCES

Chen, J., Owen, J.M. and Wilson, M., 1993a. Parallel-computing techniques applied to rotor-stator systems: fluid dynamics computations, in Numerical Methods in Laminar and Turbulent Flow, 8, 899 - 911, Pineridge Press, Swansea.

Chen, J., Owen, J.M. and Wilson, M., 1993b. Parallel-computing techniques applied to rotor-stator systems: thermal computations, in Numerical Methods in Thermal Problems, 8, 1212 - 1226, Pineridge Press, Swansea.

Chen, J-X., Gan, X. and Owen, J.M., 1996. Heat transfer in an air-cooled rotor-stator system. J.Turbomachinery, 118, 444 – 451.

El-Oun, Z and Owen, J.M., 1989. Pre-swirl blade-cooling effectiveness in an adiabatic rotor-stator system. J. Turbomachinery, 111, 522 - 529.

Karabay, H., Chen, J-X., Pilbrow, R., Wilson, M. and Owen, J.M., 1997. Flow in a cover-plate pre-swirl rotor-stator system. ASME Int. Gas Turbine and Aeroengine Congress, Orlando, June 1997. ASME Paper No 97-GT-243 (to be published in TransASME).

Launder, B.E. and Sharma, B.I., 1974. Application of the energy dissipation model of turbulence to flow near a spinning disc, Letters in Heat and Mass Transfer, 1, 131-138.

Meierhofer, B. and Franklin, C.J., 1981. An investigation of a preswirled cooling airflow to a gas turbine disk by measuring the air temperature in the rotating channels. ASME Int. Gas Turbine Conf., Houston, Paper No 81-GT-132.

Morse, A.P., 1988. Numerical prediction of turbulent flow in cavities. J.Turbomachinery, 110, 202-215.

Owen, J.M. and Rogers, R.H., 1989. Flow and heat transfer in rotating-disc systems, Vol.1: Rotor-stator systems. Research Studies Press, Taunton. (John Wiley, New York).

Owen, J.M. and Rogers, R.H., 1995. Flow and heat transfer in rotating-disc systems, Vol.2: Rotating Cavities. Research Studies Press, Taunton (John Wiley, New York).

Popp, O., Zimmermann, H., and Kutz, J., 1996. CFD analysis of coverplate receiver flow. ASME Int. Gas Turbine and Aeroengine Cong., Birmingham, UK. Paper No 96-GT-357.

Wilson, M., Pilbrow, R.G. and Owen, J.M., 1997. Flow and heat transfer in a pre-swirl rotor-stator system. J.Turbomachinery, 119, 364-373.